Supplement of Atmos. Chem. Phys., 20, 10063–10072, 2020
https://doi.org/10.5194/acp-20-10063-2020-supplement

Atmospheric Chemistry and Physics
Open Access
EGU

Supplement of

The value of remote marine aerosol measurements for constraining radiative forcing uncertainty

Leighton A. Regayre et al.

Correspondence to: Leighton A. Regayre (l.a.regayre@leeds.ac.uk) and Julia Schmale (julia.schmale@psi.ch)

SI Methods

SI Methods: Model Version

We use the Global Atmosphere 4 (GA 4.0; Walters et al., 2014) configuration of the Hadley Centre General Environment Model version 3 (HadGEM3; Hewitt et al., 2011), which incorporates the UK Chemistry and Aerosol (UKCA) model at version 8.4 of the UK Met Office's Unified Model (UM). UKCA simulates trace gas chemistry and the evolution of the aerosol particle size distribution and chemical composition using the GLObal Model of Aerosol Processes (GLOMAP-mode; Mann et al., 2010) and a whole-atmosphere chemistry scheme (Morgenstern et al., 2009; O'Connor et al., 2014). The model has a horizontal resolution of 1.25x1.875 degrees and 85 vertical levels. The aerosol size distribution is defined by seven log-normal modes: one soluble nucleation mode as well as soluble and insoluble Aitken, accumulation and coarse modes. The aerosol chemical components are sulfate, sea salt, black carbon (BC), organic carbon (OC) and dust. Secondary organic aerosol (SOA) material is produced from the first stage oxidation products of biogenic monoterpenes under the assumption of zero vapour pressure and is combined with primary particulate organic matter after kinetic condensation. Use of the GLOMAP model to simulate aerosol size and composition changes reduces Southern Ocean radiative biases in HadGEM3 (Bodas-Salcedo et al., 2019).

GLOMAP simulates new particle formation, coagulation, gas-to-particle transfer, cloud processing and deposition of gases and aerosols. The activation of aerosols into cloud droplets is calculated using globally prescribed distributions of sub-grid vertical velocities (West et al. 2014) and the removal of cloud droplets by autoconversion to rain is calculated by the host model. Aerosols are also removed by impaction scavenging of falling raindrops according to the collocation of clouds and precipitation (Lebsock et al., 2013; Boutle et al., 2014). Aerosol water uptake efficiency is determined by kappa-Kohler theory (Petters and Kreidenweis, 2007) using composition-dependent hygroscopicity factors.

We prescribe anthropogenic emissions using the emission inventory prepared for the Atmospheric Chemistry and Climate Model Inter-comparison Project (ACCMIP) and also prescribed in some of the CMIP Phase 5 experiments. Present-day carbonaceous aerosol emissions were prescribed using a ten year average of 2002 to 2011 monthly mean data from the Global Fire and Emissions Database (GFED3; van der Werf et al., 2010) and according to Lamarque et al. (2010) for 1850. We prescribe volcanic SO_2 emissions for continuously emitting and sporadically erupting volcanoes (Andres et al., 1998) and for explosive volcanic eruptions (Halmer et al., 2002). Surface ocean dimethyl-sulfide concentrations are prescribed using Kettle and Andreae (2000) and emitted into the atmosphere using a surface wind speed dependent parametrisation (following Nightingale et al., 2000). Sea spray is emitted into the atmosphere using the Gong (2003) surface wind speed dependent parametrisation.

Several modifications were made to version 8.4 of UKCA to overcome known structural deficiencies in the model. An organically-mediated boundary layer nucleation parametrisation (Metzger et al., 2010) was included so that remote marine and early-industrial aerosol concentrations were not unrealistically low in the model. We also added a parametrisation for ice crystal suppression of precipitation known to bring remote marine aerosol concentrations in line with measurements (Browse et al., 2012). Dust in the base model is calculated using the CLASSIC bin scheme (Woodward et al., 2001), which we replaced in our model version so that dust is emitted using the GLOMAP modal scheme. This means interactions between dust and other aerosols are explicitly simulated. We better resolve the optical properties of aerosols across wavelengths by improving the resolution of the default look-up tables. Finally, we made minor adjustments to some process parametrisations so that parameter values could be perturbed globally. All changes to the model are described fully in Yoshioka et al. (2019).

SI Methods: Perturbed Parameter Ensembles

We make use of the AER and AER-ATM perturbed parameter ensembles (PPEs) described in Yoshioka et al. (2019). Results in the main article make use of the AER PPE except for the quantification of aerosol ERF and its components. These two PPEs were designed to provide complementary insights into causes of uncertainty in the climate system. The 235 member AER PPE samples uncertainties in a set of 26 aerosol parameters, whilst the 191 member AER-ATM PPE samples uncertainties in 18 aerosol and 9 physical atmosphere parameters related

to clouds, radiation and moisture. The effects of rapid atmospheric adjustments to aerosols are not included in AER, but are included in AER-ATM (although they have a relatively minor impact on aerosol forcing in this model (e.g. Mulcahy et al., 2018). Therefore, ERF is calculated for the AER-ATM PPE and combined (in the "SI Results: Additional constraint to achieve radiative balance" section) with the CERES top-of-the-atmosphere constraint employed in Regayre et al. (2018), whilst RF is calculated for the AER PPE and combined (in the main article) with the predominantly Northern Hemisphere aerosol constraint employed in Johnson et al. (2019).

Both PPEs were nudged towards European Centre for Medium-Range Weather Forecasts (ECMWF) ERA-Interim reanalyses. Nudging means that pairs of simulations have near-identical synoptic-scale features, which enables the effects of parameter perturbations to be quantified using single-year simulations, although the magnitude of forcing will vary with the chosen year (Yoshioka et al., 2019; Fiedler et al., 2019). We nudge well above the Earth's surface in order to strike a balance between the computational cost of perturbing multiple parameters and the computational saving of using prescribed meteorology to overcome internal variability (Zhang et al., 2016). In the AER-ATM PPE only horizontal winds above the boundary layer (around 2km) for the year 2006 were prescribed, whilst in AER, horizontal winds and temperatures for 2008 were prescribed above around 1km. In each PPE the model was allowed to respond to parameter perturbations (a spin-up period) prior to simulating the data used here. Despite these differences, results in the main article are consistent across the PPEs.

SI Methods: Sampling and uncertainty

We sample uncertainty in model output using uniform pdfs across each parameter range. The uncertainty in individual parameters could be sampled in a more informed manner. For example, Yoshioka et al. (2019) used expert elicited information about likely parameter values to create parameter pdfs, which were used by Bellouin et al. (2019) and Watson-Paris et al. (2020) to sample uncertainty in aerosol forcing uncertainty. The additional information provided by expert elicited parameter pdfs is invaluable for quantifying the causes of model uncertainty (e.g. Regayre et al., 2018) because the choice of pdfs affects the contributions to variance in model output. However, in nearly 30 dimensions, samples of combined parameter values using multiple pdfs with centralised tendencies will be heavily weighted towards the centre of the parameter space. Since our intention in this article is to sample the range of model behaviour in response to the full spectrum of uncertain parameter combinations prior to constraint using measurements, we use uniform pdfs with maximum and minimum values from the expert elicited ranges.

A set of around 200 model variants that make up the PPEs are much too small to allow statistical analysis of model performance across nearly 30 dimensions of parameter space. We therefore use output from the PPEs to train Gaussian Process emulators (e.g. Lee et al., 2012), which define how the model outputs vary continuously over the parameter space. Some additional uncertainty is caused by emulating (rather than simulating) model output and this uncertainty is incorporated into our model-measurement constraint process (SI Methods: Model-measurement comparisons), despite being much smaller than other sources of uncertainty (Johnson et al., 2019). We sample Monte Carlo points from the emulated parameter space to produce the set of one million model variants.

SI Methods: Measurements

Measurements were collected during the ACE-SPACE campaign between December 2016 and March 2017. The measurement methodology is explained in Schmale et al. (2019) as well as in the metadata of the datasets cited below. We constrain the model uncertainty using near-surface measurements of cloud condensation nuclei concentrations at 0.2% and 1.0% supersaturations ($CCN_{0.2}$ and $CCN_{1.0}$; Tatzelt et al., 2019), as well as number concentrations of particles with dry aerodynamic diameter larger than 700 nm (N_{700}; corresponds to volume equivalent diameter larger than around 500 to 570 nm; Schmale et al., 2019a) and mass concentrations of non-sea-salt sulfate in PM_{10}. We compare simulated and measured $CCN_{0.2}$ concentrations because cloud-active aerosol concentrations are fundamentally important for RF_{aci}. We use $CCN_{1.0}$ measurements to challenge the model's ability to reproduce concentrations of relatively small aerosols that only activate to form cloud droplets at very high supersaturations. We target the highly uncertain sea spray emission flux scaling parameter by comparing concentrations of N_{700} to simulated concentrations of sea spray aerosol, approximated using our model's soluble accumulation and coarse mode aerosol concentrations (Mann et al., 2010). This is not a like-for-like comparison because our soluble accumulation mode includes aerosols with dry diameter larger than 100 nm (Mann et al., 2010; rather than around 500 to 570 nm). Additionally, our soluble accumulation and coarse modes include negligible contributions from sulfate, primary organic matter and aged carbonaceous and dust particles.

However, over the Southern Ocean we think it is safe to assume that sea spray is the predominant (if not only) source of relatively large aerosols. Finally, we compare non-sea-salt sulfate concentrations (which omit primary sulfate in sea spray aerosol) in order to constrain the uncertainty in the emission flux of dimethyl-sulphide from the ocean surface. The sea salt fraction of sulfate was calculated using sodium as a tracer for the enrichment of sea salt in the aerosol phase (Sander et al., 2003). Non-sea-salt sulfate was calculated by subtracting this fraction from the total particulate sulfate as detected from PM_{10} filters.

Data for all variables were averaged for comparison with monthly mean model values by taking the mean of all data points that were collected at locations corresponding to positions within model gridboxes. This spatial and temporal degradation introduces representation errors that we account for using our model-measurement comparison (next section). However, the reduction in data volume makes the model-measurement comparison over one million model variants tractable.

We present monthly mean and annual cloud droplet number concentrations in Table 1 from the model and from satellite data, over the region between 50°S and 60°S. Following Grosvenor et al., (2018), we calculated cloud droplet concentrations from the MODIS (MODerate Imaging Spectroradiometer) Collection 5.1 Joint Level-2 (Aqua satellite) for the year 2008 (to correspond to the meteorological year used in our simulations). Our calculation used cloud optical depth and 3.7 micron effective radius values derived under the adiabatic cloud assumption (essentially, cloud liquid water increases linearly with height, droplet concentrations are constant throughout the cloud and the ratio of volume mean radius to effective radius is constant). We improved the cloud droplet concentration data (Grosvenor and Wood, 2018) by excluding 1x1 degree data points for which the maximum sea-ice areal coverage over a moving 2-week window exceeded 0.001%. The sea-ice data used in this process were the daily 1x1 degree version of Cavalieri et al. (2016). As with other data used in our model-measurement comparison, we degraded the cloud droplet number concentration data to the model gridbox and monthly mean spatial and temporal resolutions.

SI Methods: Model-measurement comparisons

Our constraint approach follows Johnson et al. (2019) and involves comparing output from model variants (parameter combinations) to a set of measurements and ruling out variants that are judged to be implausible. This method uses the statistical methodology of history matching, which has been effectively applied to complex models in a range of fields (Craig et al., 1997; Williamson et al., 2013; McNeall et al., 2016; Rodrigues et al., 2017 and Andrianakis et al., 2017). We account for emulator uncertainty, measurement uncertainty (instrument error) and representativeness uncertainties (caused by spatial and temporal mismatches in resolution and sampling between model and measurements). We do not include potential structural errors (e.g. from missing processes) in our constraint approach because such errors cannot be robustly quantified a priori.

For each measurement we calculate a 'measure of implausibility' for each of the one million model variants, calculated as the model-measurement difference standardised by the combined emulator, measurement and representativeness uncertainties. Using this 'implausibility measure' we can identify implausible model variants and rule out implausible parts of parameter space via the combination of the 'closeness' of the measurement and model output, and the size of the related uncertainties. The 'implausibility metric' is defined as:

$$I(\boldsymbol{x}) = \frac{|\, M - O \,|}{\sqrt{[Var(M) + Var(O) + Var(R)]}}, \quad (1)$$

where *M* is the model variant output and *O* is the observed value (the measurement). In the denominator *Var(M)* is the variance in the model estimate (caused by emulator uncertainty), *Var(O)* is the variance in the measurement (i.e., instrument or retrieval uncertainty) and the representativeness error, *Var(R)*, is the variance associated with comparing model output to measurements at different spatial (Schutgens et al., 2016a; Weigum et al. 2016, Schutgens et al., 2017) and temporal (Schutgens et al., 2016b; Schutgens et al., 2017) resolutions. We compare the 2016-17 measurements to the models nudged towards 2008 meteorology for AER and 2006 meteorology for AER-ATM because the measurements were not collected when the PPE was created. The *Var(R)* term therefore includes additional uncertainty due to inter-annual variability. According to the definition of the implausibility measure, model variants will not be ruled out if either the model-measurement difference is small or the uncertainty in the denominator is large. In other words, we retain model variants that are skilful and model variants whose skill cannot be adequately determined because the model-measurement comparison uncertainties are too large.

The variance terms in the denominator of Eq. (1) are calculated uniquely for each measurement. Following Johnson et al. (2019), we use an instrument error of 10%, a spatial co-location uncertainty of 20% and a temporal co-location uncertainty of 10%. Fig. S1 shows an example of the degradation of data for comparison with monthly mean model output. Emulator uncertainty is calculated for each model-measurement combination using the error on the predicted mean from the emulator for the model variant. We use residuals in de-trended monthly mean output from a HadGEM-UKCA hindcast simulation over the period of 1980-2009 (Turnock et al., 2015) to estimate the inter-annual variability for each variable across all model gridboxes and months.

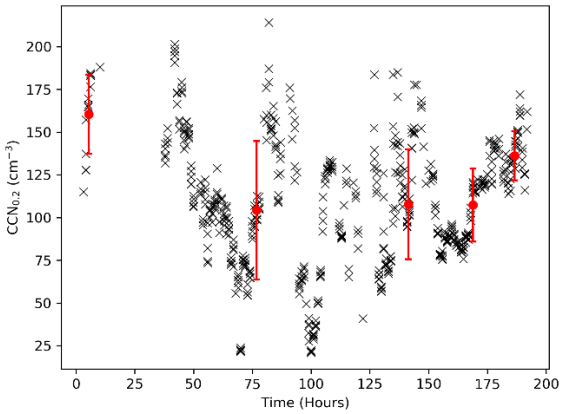

Fig S1: Measured $CCN_{0.2}$ values between the 3rd and 10th January 2017, after filtering for possible ship stack contamination. The ACE-SPACE vessel transited through 5 model gridboxes during this period. We average all measurements collected in locations, over one or more days, within each model gridbox, for comparison with monthly mean model output. These average values and one standard deviation of the measurement data are shown in red at the central time for each measurement subset. From left to right, these values correspond to the five model gridboxes in Fig. 1 between around 60ºE and 90ºE, at the following latitude and longitudes: 1) 49.5ºS, 65.5ºE, 2) 49.5ºS, 69.5ºE, 3) 54ºS, 77ºE, 4) 54ºS, 84.5ºE and 5) 56.5ºS, 92ºE.

We calculate implausibility values for each of the one million model variants for every measurement. Deciding which model variants to retain would be trivial were we comparing the sample output to a single measurement. We would sequentially rule out the variant with the highest implausibility metric until some small fraction of the original sample remained. However, our task is more complex. We need to rule out model variants based on multiple implausibility metrics that are distinct for each measurement location and measurement type.

A variant may compare well with a measurement type in one location and poorly in another because spatial and temporal features in the measurement data (e.g. changing aerosol sources) mean each measurement could provide different information about the plausibility of the models. To avoid prematurely ruling out model variants based on a few poor comparisons, we only rule out variants if their implausibility exceeds a defined threshold for more than a tolerable fraction of measurements. We choose threshold and tolerance values with a goal of retaining around 3% of the original sample. The subjective choice of 3% retention determines the results to some extent. Retaining a much smaller percentage of the model variants could potentially over-constrain the model. However, retaining a larger proportion risks weakening the constraint and retaining addition implausible variants.

We set threshold and tolerance values for each variable distinctly for each month of data. This makes processing the implausibility data more efficient and allows for a degree of automation of the constraint process. We ensure that each measurement type on each leg of the journey (Schmale et al., 2019) affects the combined constraint. This requires quantification of the constraint of individual measurement types on parameter values at multiple combinations of threshold and implausibility exceedance tolerances. We avoid increasing the threshold and/or tolerance values in individual months for each measurement type, if the constraint efficacy of the measurement would saturate as a result. Otherwise, threshold and tolerances for each month are required to be as similar as possible.

Although our analysis in the main article focusses on a combined measurement constraint, this analysis is informed by individual measurement type constraints. The threshold and exceedance tolerances for individual measurement type constraints are summarised in Table S1. Only 0.004% of the one million model variants (40 variants) are retained when these individual constraints are combined. Thus, we relax the threshold and tolerance criteria for each measurement type constraint when combining constraints (Table S2).

Table S1: Individual measurement type constraint threshold values and exceedance tolerance values for December to April, as well as the percentage of the one million member sample retained by each constraint. Exceedance tolerances values are percentages of the number of measurements in each month.

	$CCN_{0.2}$	$CCN_{1.0}$	Nss-sulfate	N_{700}
Implausibility Threshold	3.5	3.5	3.5	3.5
Exceedance tolerance (%) Dec-Apr	15,15,20,20,10	2,2,2,5,2	15,20,20,15	20,20,25,20,20
Percentage retained	3.3	3.0	6.2	3.0

Table S2: Threshold values and exceedance tolerance values for December to April, as well as the percentage of the one million member sample retained by each constraint. Exceedance tolerances values are percentages of the number of measurements in each month. These constraints are combined to retain around 3% of the one million member sample of model variants, as described in the main article.

	$CCN_{0.2}$	$CCN_{1.0}$	Nss-sulfate	N_{700}
Implausibility Threshold	4.5	4.5	4.0	4.5
Exceedance tolerance (%) Dec-Apr	30,30,30,30,10	25,30,30,15,5	20,20,20,15	25,25,25,30,25
Percentage retained	20.6	18.1	29.9	24.2

SI Results

SI Results: Constrained marginal parameter distributions

In Fig. 3 of the main article we show the marginal probability distributions for the 26 parameters in the AER PPE. These marginal distributions show the effect of measurement constraint on individual parameter likelihoods. Marginal densities for the constrained sample are scaled such that the tops of the constrained and unconstrained pdfs are aligned. Similar parameter constraints are found when constraining the AER-ATM PPE using the same constraint process and original set of measurements (Fig. S2). In addition to parameters that are perturbed in both PPEs, we show the effect of measurement constraint on the few physical atmosphere parameters (Rad_Mcica_Sigma and Fac_Qsat) that are constrained by our process as well as additional aerosol parameters that were perturbed in AER-ATM (BC_RI and OC_RI).

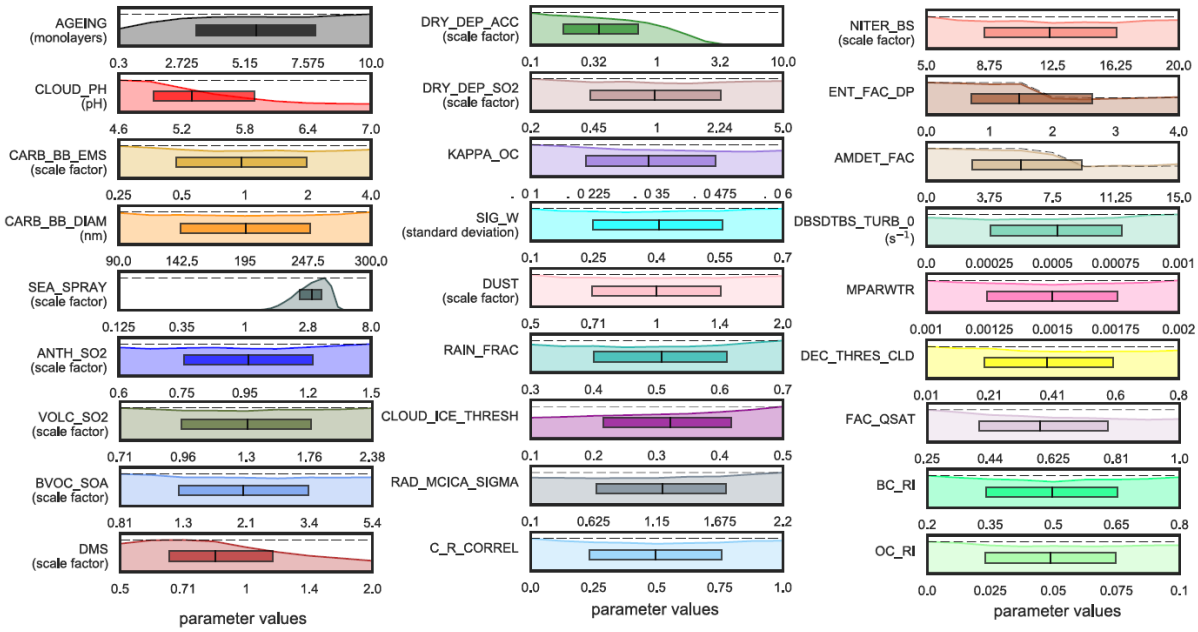

Fig. S2. Marginal probability distributions for aerosol and physical atmosphere parameters from the AER-ATM PPE after constraint. The density of parameter values in the unconstrained sample are shown as dashed lines. Densities of constrained samples are shown in colour. The 25th, 50th and 75th percentiles of each marginal distribution are shown in the central boxes. Parameter values on the x-axes correspond to values used in the model (Yoshioka et al., 2019).

In addition to the constraint achieved by combining remote marine aerosol measurements, Table S3 shows the effect of individual measurement type constraints (Table S2) on model parameters and how these translate into a combined constraint (Fig. 3).

Table S3. Ranges and inter-quartile ranges of marginal parameter distributions from individual constraints using measured concentrations of $CCN_{0.2}$, $CCN_{1.0}$, non-sea-salt sulfate and N_{700}, as well as for the combined constraint. These individual constraints are those described in Table S2 and were combined to constrain the model and make Fig. 3. Values are marked in bold where the individual measurement type constraint moves the range, 25th or 75th percentile closer towards the range or percentiles of the combined constraint than other measurement types, relative to the unconstrained values.

Parameter Name	Unconstrained	$CCN_{0.2}$	$CCN_{1.0}$	Non-sea-salt sulfate	N_{700}	Combined
BL_Nuc	0.1,10.0 [0.3,3.2]	0.1,10.0 [0.3,**3.5**]	0.1,10.0 [0.3,3.0]	0.1,10.0 [0.3,3.3]	0.1,10.0 [0.3,3.2]	0.1,10.0 [0.3,3.5]
Ageing	0.3,10.0 [2.7,7.6]	0.3,10.0 [3.0,7.9]	0.3,10.0 [2.5,7.5]	0.3,10.0 [2.7,7.6]	0.3,10.0 [2.6,7.5]	0.3,10.0 [2.7,7.6]
Acc_ Width	1.2,1.8 [1.4,1.6]	1.2,1.8 [**1.3**,1.7]	1.2,1.8 [1.4,1.7]	1.2,1.8 [1.4,1.7]	1.2,1.8 [**1.3**,1.7]	1.2,1.8 [1.3,1.7]
Ait_Width	1.2,1.8 [1.3,1.6]	1.2,1.8 [1.3,1.7]	1.2,1.8 [1.3,1.6]	1.2,1.8 [1.3,1.7]	1.2,1.8 [1.3,1.7]	1.2,1.8 [1.3,1.6]
Cloud_pH	4.6,7.0 [5.2,6.4]	4.6,7.0 [**5.1**,6.4]	4.6,7.0 [**5.1**,**6.2**]	4.6,7.0 [5.2,6.4]	4.6,7.0 [5.2,6.4]	4.6,7.0 [5.1,6.2]
Carb_FF_ Ems	0.5,2.0 [0.7,1.4]	0.5,2.0 [0.7,1.4]	0.5,2.0 [0.7,1.4]	0.5,2.0 [0.7,1.4]	0.5,2.0 [0.7,1.4]	0.5,2.0 [0.7,1.4]
Carb_BB_ Ems	0.25,4.00 [0.50,2.00]	0.25,4.00 [0.52,**2.16**]	0.25,4.00 [**0.48**,2.01]	0.25,4.00 [0.50,2.01]	0.25,4.00 [0.49,2.03]	0.25,4.00 [0.49,2.06]
Carb_Res_ Ems	0.25,4.00 [0.50,2.00]	0.25,4.00 [**0.45**,**1.78**]	0.25,4.00 [0.48,2.02]	0.25,4.00 [0.49,2.00]	0.25,4.00 [0.50,2.02]	0.25,4.00 [0.48,1.94]
Carb_FF_ Diam	30,90 [45,75]	30,90 [45,**76**]	30,90 [44,75]	30,90 [45,75]	30,90 [45,75]	30,90 [45,76]
Carb_BB_ Diam	90,300 [143,248]	90,300 [141,**250**]	90,300 [**140**,249]	90,300 [142,248]	90,300 [141,248]	90,300 [141,249]
Carb_Res_ Diam	90,500 [193,398]	90,500 [193,**404**]	90,500 [**190**,399]	90,500 [192,400]	90,500 [193,400]	90,500 [189,400]
Prim_SO4_ Frac	1.0e-6,1.0e-1 [1.8e-5,5.6e-3]	1.0e-6,1.0e-1 [1.7e-5,6.5e-3]	1.0e-6,1.0e-1 [**1.3e-5**,**4.2e-3**]	1.0e-6,1.0e-1 [1.7e-5,5.6e-3]	1.0e-6,1.0e-1 [1.6e-5,6.0e-3]	1.0e-6,1.0e-1 [1.6e-5,5.2e-3]
Prim_SO4_ Diam	3,100 [27,76]	3,100 [26,**75**]	3,100 [**29**,**78**]	3,100 [27,76]	3,100 [26,77]	3,100 [28,77]
Sea_ Spray	0.1,8.0 [0.4,2.8]	1.5,8.0 [2.7,3.8]	**1.9**,8.0 [**3.8**,**5.7**]	0.1,8.0 [0.3,2.8]	1.5,**5.2** [2.5,3.6]	1.6,5.1 [2.6,3.7]
Anth_SO2	0.6,1.5 [0.8,1.2]	0.6,1.5 [0.8,1.2]	0.6,1.5 [0.7,1.2]	0.6,1.5 [0.8,1.2]	0.6,1.5 [0.8,1.2]	0.6,1.5 [0.8,1.2]
Volc_SO2	0.7,2.4 [1.0,1.8]	0.7,2.4 [1.0,1.8]	0.7,2.4 [1.0,1.8]	0.7,2.4 [1.0,1.8]	0.7,2.4 [1.0,1.8]	0.7,2.4 [1.0,1.8]
BVOC_ SOA	0.8,5.4 [1.3,3.4]	0.8,5.4 [1.3,3.5]	0.8,5.4 [1.4,3.5]	0.8,5.4 [1.3,3.4]	0.8,5.4 [1.3,3.4]	0.8,5.4 [1.3,3.4]
DMS	0.5,2.0 [0.7,1.4]	0.5,2.0 [0.7,1.5]	0.5,2.0 [0.7,1.4]	0.5,2.0 [**0.8**,1.5]	0.5,2.0 [0.7,1.4]	0.5,2.0 [0.8,1.3]
Dry_Dep_ Ait	0.5,2.0 [0.7,1.4]	0.5,2.0 [0.7,1.4]	0.5,2.0 [0.7,1.3]	0.5,2.0 [0.7,1.4]	0.5,2.0 [0.7,1.4]	0.5,2.0 [0.7,1.4]
Dry_Dep_ Acc	0.1,10.0 [0.3,3.2]	0.1,9.3 [**0.2**,**0.9**]	0.1,**6.7** [**0.2**,1.0]	0.1,10.0 [0.3,1.9]	0.1,10.0 [0.3,3.2]	0.1,6.4 [0.2,0.8]
Dry_Dep_ SO2	0.2,5.0 [0.4,2.2]	0.2,5.0 [0.4,2.2]	0.2,5.0 [0.4,2.4]	0.2,5.0 [0.4,2.2]	0.2,5.0 [0.4,2.2]	0.2,5.0 [0.4,2.2]
Kappa_ OC	0.1,0.6 [0.2,0.5]	0.1,0.6 [0.2,0.5]	0.1,0.6 [0.2,0.5]	0.1,0.6 [0.2,0.5]	0.1,0.6 [0.2,0.5]	0.1,0.6 [0.2,0.5]
Sig_W	0.1,0.7 [0.3,0.5]	0.1,0.7 [0.2,0.6]	0.1,0.7 [0.2,0.6]	0.1,0.7 [0.2,0.6]	0.1,0.7 [0.2,0.6]	0.1,0.7 [0.2,0.6]

Dust	0.5,2.0 [0.7,1.4]	0.5,2.0 [0.7,1.4]	0.5,2.0 [0.7,1.4]	0.5,2.0 [0.7,1.4]	0.5,2.0 [0.7,1.4]	0.5,2.0 [0.7,1.4]
Rain_Frac	0.3,0.7 [0.4,0.6]	0.3,0.7 [0.4,0.6]	0.3,0.7 [0.4,0.6]	0.3,0.7 [0.4,0.6]	0.3,0.7 [0.4,0.6]	0.3,0.7 [0.4,0.6]
Cloud_Ice_ Thresh	0.1,0.5 [0.2,0.4]	0.1,0.5 [0.2,**0.3**]	0.1,0.5 [0.2,0.4]	0.1,0.5 [0.2,0.4]	0.1,0.5 [0.2,0.4]	0.1,0.5 [0.2,0.4]

Constrained marginal parameter distributions in Fig. 3 and Fig. 5 of the main article tell a one-dimensional story. In Fig. S3, we show the effect of constraint to remote marine aerosol measurements, combined with the constraint from Johnson et al. (2019) on a subset of the marginal 2-dimensional parameter combinations.

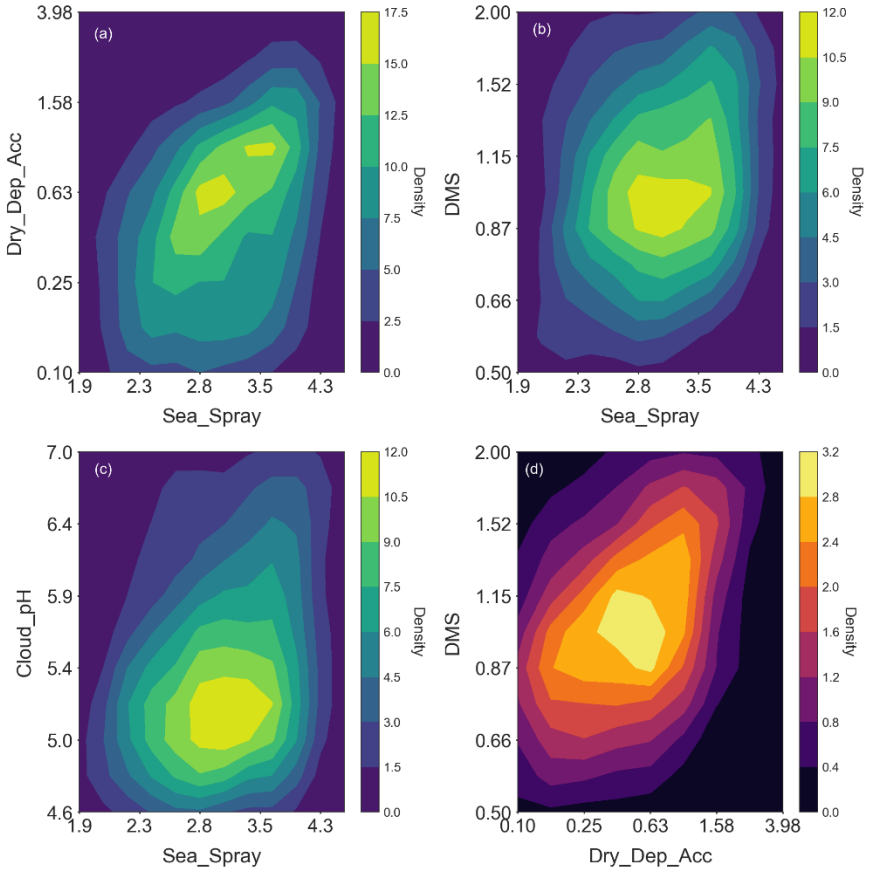

Fig. S3. Two-dimensional marginal probability density distributions for a) sea spray emission flux scale factor (Sea_Spray) and the Accumulation aerosol mode dry deposition velocity scale factor (Dry_Dep_Acc), b) sea spray emission flux scale factor and dimethylsulfide surface water concentration scale factor (DMS), c) sea spray emission flux scale factor and cloud droplet pH (Cloud_pH), and d) Accumulation aerosol mode dry deposition velocity scale factor and dimethylsulfide surface water concentration scale factor. Individual parameter ranges are plotted according to their constrained values (Table S3), not the full range of values used in the original sample of model variants as shown in Fig. 3, Fig. 5 and Fig. S2.

SI Results: Wind Speed discrepancies

Southern Ocean wind speeds during the ACE-SPACE expedition were often much lower than climatological mean values, but on average were higher than winds in our ensemble (Schmale et al., 2019). We account for the effects of inter-annual variability in the Var(R) term in equation S1. However, monthly mean differences between ERA-Interim wind speeds in the measurement year and the year used in the ensemble are less than 20% along the route taken by the ACE-SPACE campaign vessel (Fig. S4). The modest discrepancy in wind speeds may be important for constraining aerosol concentrations, because sea spray emissions in our model are strongly dependent on wind speeds (Gong, 2003). However, the measured wind speed and N700 values are only weakly correlated (Pearson correlation coefficient of around 0.2) when degraded to the resolution used for comparison with model output.

Our constraint process has in-built functionality that prevents the use of measurements with large model-measurement discrepancies. We tested the robustness of our constraint methodology to the discrepancy in wind

speeds by neglecting around 50% of the measurements (those with the largest discrepancies between measured and AER-ATM PPE mean simulated winds) and repeating the constraint. The effects on marginal parameter and aerosol forcing constraints were negligible (not shown). The consistency of constraint, with and without measurements in locations with relatively large model-measurement wind speed discrepancies, suggests the constraint methodology is insensitive to wind speed discrepancies caused by daily wind speed variability and differences in meteorological years between model simulations and measurements.

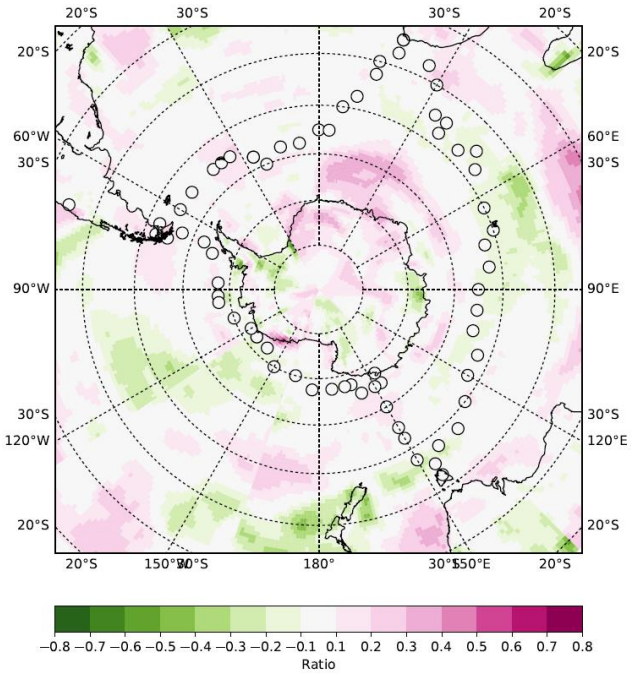

Fig. S4. Ratio of ERA-Interim wind speed differences (between measurement and simulated years) to the measurement year. Monthly mean winds from 2006 (matching the AER PPE) were subtracted from monthly mean winds for December 2016 to April 2017 (matching the ACE-SPACE campaign) to calculate the differences. The map is an assimilation of data between months, where data is presented at each location for months corresponding to the timing of the ACE-SPACE measurement campaign.

SI Results: Effect of constraint on cloud droplet number concentration

Table 1 shows that our constraint on natural emission parameters also constrains summertime Southern Ocean cloud droplet number concentrations towards higher values. Credible interval ranges are reduced by around 50% and mean values are in closer agreement with MODerate Imaging Spectroradiometer (MODIS; Salomonson et al., 1989) instrument data (note that droplet number concentrations were not used to constrain the model). Thus, we conclude in the main article that the constraint on aerosol forcing towards weaker values is a genuine constraint, associated with higher cloud droplet number concentrations, increased aerosol load and higher natural aerosol emissions, and is not the result of an arbitrary tuning.

SI Results: Additional constraint to achieve radiative balance

We additionally test the effect of ruling out model variants that differ from the Clouds and the Earth's Radiant Energy System (CERES; Loeb et al., 2009) measurement of global, annual mean top-of-the-atmosphere outgoing shortwave radiative flux of 98.3 W m^{-2} by more than 0.25 W m^{-2}, which was the constraint applied in Regayre et al. (2018). The constraint on ERF using the CERES-derived top-of-the-atmosphere fluxes in addition to the ACE-SPACE measurement dataset weakens the reduction in aerosol ERF from 8% to 7%. Fig. S5 (for comparison with Fig. 4a) shows the effect of this additional constraint on aerosol ERF. Retaining only model variants that agree with top-of-the-atmosphere radiative flux measurements does not noticeably affect the constraint on aerosol ERF (as shown in Regayre et al., 2018). Furthermore, the marginal parameter pdfs are unaffected by the additional constraint (not shown).

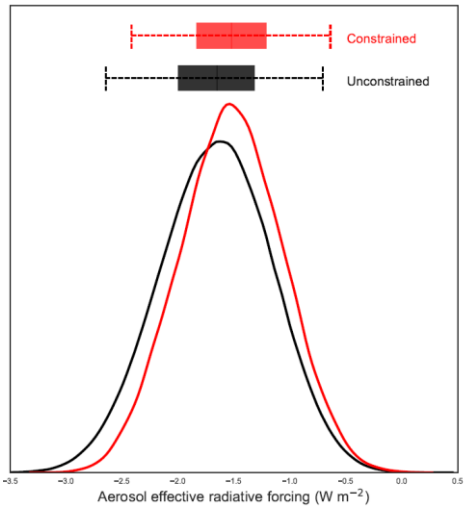

Fig. S5. Probability distribution of ERF_{aci} from the AER-ATM PPE. Values from the unconstrained sample of one million model variants are in black. Red lines show the values constrained by ACE-SPACE measurements and additionally constrained using CERES top-of-the-atmosphere measurements. Plotting features are identical to Fig. 4.

SI References:

Adrianakis, I., Vernon, I., McCreesh, N., McKinley, T. J., Oakley, J. E., Nsubuga, R. N., Goldstein, M., and White, R. G.: History matching of a complex epidemiological model of human immunodeficiency virus transmission by using variance emulation, J. Roy. Stat. Soc. C-App., 66, 717–740, doi:10.1111/rssc.12198, 2017.

Andreae, M. O., Jones, C. D., and Cox, P. M.: Strong present-day aerosol cooling implies a hot future, Nat., 435, 1187–1190, doi:10.1038/nature03671, 2005.

Andres, R. J. and Kasgnok, A. D.: A time-averaged inventory of subaerial volcanic sulfur emissions, J. Geo. Res., 103, 25 251–25 262, doi:10.1029/98JD02091, 1998.

Bellouin, N. Quaas, J., Gryspeerdt, E., Kinne, S., Stier, P., Watson-Paris, D., Boucher, O., Carslaw, K.C., Christensen, M., Daniau, A.-L., Dufresne, J.-L., Feingold, G., Fiedler, S., Forster, P., Gettleman, A., Haywood, J.M., Lohmann, U., Malavelle, F., Mauritsen, T., McCoy, D.T., Mhyre, G., Mülmenstädt, J., Neubauer, D., Possner, A., Rugenstein, M., Sato, Y., Schulz, M., Schwartz, S.E., Sourdeval, O., Storelvmo, T., Toll, V., Winker, D. and Stevens, B.: Bounding global aerosol radiative forcing of climate change, Rev. Geophys., 58, e2019RG000660, doi:10.1029/2019RG000660, 2019.

Bodas-Salcedo, A., Mulcahy, J. P., Andrews, T., Williams, K. D., Ringer, M. A., Field, P. R., and Elsaesser, G. S.: Strong dependence of atmospheric feedbacks on mixed-phase microphysics and aerosol-cloud interactions in HadGEM3, J. Adv. Model. Earth Syst., 11, 1735–1758, doi:10.1029/2019MS001688, 2019.

Boutle, I. A., Abel, S. J., Hill, P. G., and Morcrette, C. J.: Spatial variability of liquid cloud and rain: observations and microphysical effects, Quart. J. Roy. Meteor. Soc., 140, 585–594, doi:10.1002/qj.2140, 2014.

Browse, J., Carslaw, K. S., Arnold, S. R., Pringle, K. J., and Boucher, O.: The scavenging processes controlling the seasonal cycle in Arctic sulphate and black carbon aerosol, Atmos. Chem. Phys., 12, 6775–6798, doi:10.5194/acp-12-6775-2012, 2012.

Carslaw, K. S., Boucher, O., Spracklen, D. V., Mann, G. W., Rae, J. G. L., Woodward, S., and Kulmala, M.: A review of natural aerosol interactions and feedbacks within the Earth system, Atmos. Chem. Phys., 10, 1701–1737, 10.5194/acp-10-1701-2010, 2010.

Carslaw, K. S., Lee, L. A., Reddington, C. L., Pringle, K. J., Rap, A., Forster, P.M.,Mann, G.W., Spracklen, D. V.,Woodhouse,M., Regayre, L. A., and Pierce, J. R.: Large contribution of natural aerosols to uncertainty in indirect forcing, Nat., 503, 67–71, doi:10.1038/nature12674, 2013.

Carslaw, K. S., Gordon, H., Hamilton, D. S., Johnson, J. S., Regayre, L. A., and Yoshioka, M.: Aerosols in the pre-industrial atmosphere, Curr. Clim. Change Rep., 3, 1–15, doi:10.101007/s40641-017-0061-2, 2017.

Cavalieri, D. J., Parkinson, C. L., Gloersen, P. and Zwally, H. J.: Sea ice concentrations from Nimbus-7 SMMR and DMSP SSM/I-SSMIS passive microwave data, Version 1., NASA National Snow and Ice Data Center Distributed Active Archive Centerm Boulder, Colorado, USA., Accessed 22nd December 2016, https://doi.org/10.5067/8gq8lzqvl0vl, 1996.

Collins, M., Knutti, R., Arblaster, J., Dufresne, J. L., Fichefet, D., Friedlingstein, P., Gao, X., Gutowski, W. J., Johns, T., Krinner, G., Shongwe, M., Tebaldi, C., Weaver, A. J., and Wehner, M.: Long-term Climate Change: Projections Commitments and Irreversibility, in: Climate Change 2013: The Physical Science Basis. Contribution of Working Group I to the Fifth Assessment Report of the Intergovernmental Panel on Climate Change, edited by Stocker, T. F., Qin, D., Plattner, G. K., Tignor, M., Allen, S. K., Boschung, J., Nauels, A., Xia, Y., Bex, V., and Midgley, P. M., Cambridge University Press, Cambridge, United Kingdom and New York, NY, USA, 2013.

Craig, P. S., Goldstein,M., Seheult, A. H., and Smith, J. A.: Pressure Matching for Hydrocarbon Reservoirs: A Case Study in the Use of Bayes Linear Strategies for Large Computer Experiments, in: Case Studies in Bayesian Statistics. Lecture Notes in Statistics, edited by Gatsonis, C., Hodges, J. S., Kass, R. E., McCulloch, R., Rossi, P., and N.D., N. D. S., Springer, New York, NY, doi:10.1007/978-1-4612-2290-3_2, 1997.

Fiedler, S., Kinne, S., Katty Huang, W. T., Räisänen, P., O'Donnell, D., Bellouin, N., Stier, P., Merikanto, J., van Noije, T., Carslaw, K. S., Makkonen, R., and Lohman, U.: Anthropogenic aerosol forcing – insights from multi-estimates from aerosol-climate models with reduced complexity, Atmos. Chem. Phys., 19, TBA, doi:10.5194/acp-2018-639, 2019.

Gong, S. L.: A parameterization of sea-salt aerosol source function for sub- and super-micron particles, Glob. Biogeochem. Cyc., 17, 1097, doi:10.1029/2003GB002079, 2003.

Grosvenor, D.P., Sourdeval, O., Zuidema, P., Ackerman, A., Alexandrov, M.D., Bennartz, R., Boers, R., Cairns, B., Chiu, J.C., Christensen, M., Deneke, H., Diamond, M., Feingold, G., Fridlind, A., Hünerbein, A., Knist, C., Kollias, P., Marshak, A., McCoy, D., Merk, D., Painemal, D., Rausch, J., Rosenfeld, D., Russchenberg, H., Seifert, P., Sinclair, K., Stier, P., van Diedenhoven, B., Wendisch, M.,, Werner, F., Wood, R., Zhang, Z. and Quaas, J.: Remote sensing of droplet number concentration in warm clouds: A review of the current state of knowledge and perspectives, Rev. Geophys., 56, 409-453, doi:10.1029/2017RG000593, 2018.

Grosvenor, D. P. and Wood, R.: Daily MODIS (MODerate Imaging Spectroradiometer) derived cloud droplet number concentration global dataset for 2003-2015., Centre for Env. Data Anal., https://catelogue.ceda.ac.uk/uuid/cf97ccc802d348ec8a3b6f2995dfbbff, 2018.

Gryspeerdt, E., Quaas, J., Ferrachat, S., Gettelman, A., Ghan, S., Lohmann, U., Morrison, H., Neubauer, D., Partridge, D. G., Stier, P., Takemura, T., Wang, H., Wang, M., and Zhang, K.: Constraining the instantaneous aerosol influence on cloud albedo, Proc. Natl. Acad. Sci., 114, 4899–4904, doi:10.1073/pnas.1617765114, 2017.

Halmer, M., Schmincke, H. U., and Graf, H. F.: The annual volcanic gas input into the atmosphere, in particular into the stratosphere: a global data-set for the past 100 years, J. Volcanol. Geotherm. Res., 115, 511–528, doi:10.1016/S0377-0273(01)00318-3, 2002.

Hamilton, D. S., Lee, L. A., Pringle, K. J., Reddington, C. L. S., Spracklen, D. V., and Carslaw, K. S.: Occurrence of pristine aerosol on a polluted planet, Proc. Natl. Acad. Sci., 111, 18 466–18 471, doi:10.1073/pnas.1415440111, 2014.

Hewitt, H. T., Copsey, D., Culverwell, I. D., Harris, C. M., Hill, R. S. R., Keen, A. B., McLaren, A. J., and Hunke, E. C.: Design and implementation of the infrastructure of HadGEM3: the next-generation Met Office climate modelling system, Geosci. Mod. Dev., 4, 223–253, doi:10.5194/gmd-4-223-2011, 2011.

Johnson, J. S., Regayre, L. A., Yoshioka, M., Pringle, K. J., Turnock, S. T., Browse, J., and Carslaw, K. S.: Robust observational constraint of processes and emissions in a climate model and the effect on aerosol radiative forcing, Atmos. Chem. Phys. Discuss., doi:10.5194/acp-2019-834, in review, 2019.

Kelle, A. J. and Andreae, M. O.: Flux of dimethylsulphide from the oceans: A comparison of updated data sets and flux models, J. Geo. Res. Atmos., 105, 26 793–26 808, doi:10.1029/2000JD900252, 2000.

Lamarque, J. F., Bond, T. C., Eyring, V., Granier, C., Heli, A., Kilmont, Z., Lee, D., Liousse, C., Mieville, A., Owen, B., Schultz, M. G., Shindell, D., Smith, S. J., Stehfest, E., Van Aardenne, J., Cooper, O. R.,

Kainuma, M., Mahowald, N., McConnell, J. R., Naik, V., Riahi, K., and van Vuuren, D. P.: Historical (1850-2000) gridded anthropogenic and biomass burning emissions of reactive gases and aerosols: methodology and application, Atmos. Chem. Phys., 10, 7017–7039, doi:10.5194/acp-10-7017-2010, 2010.

Lebsock, M., Morrison, H., and Gettleman, A.: Mircophysical implications of cloud-precipitation covariance derived from satellite remote sensing, J. Geo. Res. Atmos., 118, 6521–6533, doi:10.1001/jgrd.50347, 2013.

Lee, L. A., Carslaw, K. S., Pringle, K. J., and Mann, G. W.: Mapping the uncertainty in global CCN using emulation, Atmos. Chem. Phys., 12, 9739–9751, doi:10.5194/acp-12-9739-2012, 2012.

Lee, L. A., Reddington, C. L., and Carslaw, K. S.: On the relationship between aerosol model uncertainty and radiative forcing uncertainty, Proc. Natl. Acad. Sci., 113, 5820–5827, doi:10.1073/pnas.1507050113, 2016.

Loeb, N. G.,Wielicki, B. A., Doelling, D. R., Smith, G. L., Keyes, D. F., Kato, S., Manalo-Smith, N., and Wong, T.: Toward Optimal Closure of the Earth's Top-of-Atmosphere Radiation Budget, J. Climate., 22, 748–766, doi:10.1175/2008JCLI2637.1, 2009.

Mann, G. W., Carslaw, K. S., Spracklen, D. V., Ridley, D. A., Manktelow, P. T., Chipperfield, M. P., Pickering, S. J., and Johnson, C. E.: Description and evaluation of GLOMAP-mode aerosol microphysics model for the UKCA composition-climate model, Geosci. Mod. Dev., 3, 519–551, doi:10.5194/gmd-3-519-2010, 2010.

McCoy, D. T., Bender, F. A., Mohrmann, J. K. C., Hartmann, D. L., Wood, R., and Grosvenor, D. P.: The global aerosol-cloud first indirect effect estimated using MODIS, MERRA, and AeroCom, JGRA, 122, 1779–1796, doi:10.1002/2016JD026141, 2017.

McNeall, D., Williams, J., Booth, B. B. B., Betts, R., Challenor, P., Wiltshire, A., and D.Sexton: The impact of structural error on parameter constraint in a climate model, Ear. Sys. Dyn., 7, 917–935, doi:10.5194/esd-7-917-2016, 2016.

Metzger, A., Verheggen, B., Dommen, J., Duplissy, J., Prevot, A. S. H.,Weingartner, E., Riipinen, I., Kulmala, M., Spracklen, D. V., Carslaw, K. S., and Baltensperger, U.: Evidence for the role of organics in aerosol particle formation under atmospheric conditions, Proc. Natl. Acad. Sci., 107, 6646–6651, doi:10.1073/pnas.0911330107, 2010.

Morgenstern, O., Braesicke, P., O'Connor, F. M., Bushell, A. C., Johnson, C. E., Osprey, S. M., and Pyle, J. A.: Evaluation of the new UKCA climate-composition model – Part 1: The stratosphere, Geosci. Mod. Dev., 2, 43–57, doi:10.5194/gmd-2-43-2009, 2009.

Mulcahy, J., Jones, C., Sellar, A., Johnson, B., Boutle, I. A., Jones, A., Andrews, T., Rumbold, S. T., Mollard, J., Bellouin, N., Johnson, C. E., Williams, K. D., Grosvenor, D. P., and McCoy, D. T.: Improved aerosol processes and effective radiative forcing in HadGEM3 and UKESM1, J. Adv. Model. Earth Syst., 10, 2786—2805, doi:10.1029/2018MS001464, 2018.

Myhre, G., Shindell, D., Bréon, F. M., Collins, W., Fuglestvedt, J., Huang, J., Koch, D., Lamarque, J. F., Lee, D., Mendoza, B., Nakajima, T., Robock, A., Stephens, G., Takemura, T., and Zhang, H.: Anthropogenic and Natural Radiative Forcing, in: Climate Change 2013: The Physical Science Basis. Contribution of Working Group I to the Fifth Assessment Report of the Intergovernmental Panel on Climate Change, edited by Stocker, T. F., Qin, D., Plattner, G. K., Tignor, M., Allen, S. K., Boschung, J., Nauels, A., Xia, Y., Bex, V., and Midgley, P. M., Cambridge University Press, Cambridge, United Kingdom and New York, NY, USA, 2013.

Nightingale, P. D., Liss, P. S., and Schlosser, P.: Measurements of air-sea gas transfer during an open ocean algal bloom, Geophys. Res. Lett., 27, 2117–2120, doi:10.1029/2000GL011541, 2000.

O'Connor, F. M., Johnson, C. E., Morgenstern, O., Abraham, N. L., Braesicke, P., Dalvi, M., Folberth, G. A., Sanderson, M. G., Telford, P. J., Voulgarakis, A., Young, P. J., Zeng, G., Collins,W. J., and Pyle, J. A.: Evaluation of the new UKCA climate-composition model-Part 2: The troposphere, Geosci. Mod. Dev., 7, doi:10.5194/gmd-7-41-2014, 2014.

Petters, M. D. and Kreidenweis, S. M.: A single parameter representation of hygroscopic growth and cloud condensation nucleus activity, Atmos. Chem. Phys., 7, 1961–1971, doi:10.5194/acp-7-1961-2007, 2007.

Regayre, L. A., Pringle, K. J., Booth, B. B. B., Lee, L. A., Mann, G. W., Browse, J., Woodhouse, M. T., Rap, A., Reddington, C. L. S., and Carslaw, K. S.: Uncertainty in the magnitude of aerosol-cloud radiative forcing over recent decades, Geophys. Res. Lett., 41, 9040–9049, doi:10.1002/2014GL062029, 2014.

Regayre, L. A., Johnson, J. S., Yoshioka, M., Pringle, K. J., H.Sexton, D. M., Booth, B. B. B., Lee, L. A., Bellouin. N., and Carslaw, K. S.: Aerosols and physical atmosphere model parameters are both important sources of uncertainty in aerosol ERF, ACP, 18, 9975–10 006, doi:10.5194/acp-18-9975-2018, 2018.

Rodrigues, L. F. S., Vernon, I., and Bower, R.: Constraints on galaxy formation models from the galaxy stellar mass function and its evolution, Mon. Not. R. Astron. Soc., 466, 2418–2435, doi:10.1093/mnras/stw3269, 2017.

Salomonson, V. V., Barnes, W. L., Maymon, P. W., Montgomery, H. E. and Ostrow, H.: MODIS: advanced facility instrument for studies of the Earth as a system, in: IEEE Transactions on geoscience and remote sensing, 27, 2, 145-153, doi:10.1109/36.20292, 1989.

Sander, R., Keene, W. C., Pszenny, A. A. P., Arimoto, R., Ayers, G. P., Baboukas, E., Cainey, J. M., Crutzen, P. J., Duce, R. A., Hönninger, G., Huebert, B. J., Maenhaut, W., Mihalopoulos, N., Turekian, V. C., and Van Dingenen, R.: Inorganic bromine in the marine boundary layer: a critical review, Atmos. Chem. Phys., 3, 1301–1336, doi:10.5194/acp-3-1301-2003, 2003.

Schmale, J., Baccarini, A., Thurnherr, I., Henning, S., Efraim, A., Regayre, L. A., Bolas, C., Hartmann, M.,Welti, A., Lehtipalo, K., Aemisegger, F., Tatzelt, C., Landwehr, S., Modini, R., Tummon, F., Johnson, J. S., Harris, N., Schnaiter, M., Toffoli, A., Derkani, M., Bukowiecki, N., Stratmann, F., Dommen, J., Baltensperger, U., Wernli, H., Rosenfeld, D., Gysel-Beer, M., and Carslaw, K.: Overview of the Antarctic Circumnavigation Expedition: Study of Preindustrial-like Aerosols and Their Climate Effects (ACE-SPACE), Bull. Amer. Meteorol. Soc., 100, 11, 2260-2283, doi:10.1175/BAMS-D-18-0187.1, 2019.

Schmale, J., Henning, S., Tummon, F., Hartmann, M., Baccarini, A., Welti, A., Lehtipalo, K., Tatzelt, C., Landwehr, S. and Gysel-Beer, M.: Course mode aerosol particle size distribution collected in the Southern Ocean in the austral summer of 2016/2017, during the Antarctic Circumnavigation Expedition, Version 1.0 Dataset, doi:10.5281/zenodo.2636709, 2019a.

Schutgens, N., Gryspeerdt, E., Weigum, N., Tsyro, S., Goto, D., Schulz, M., and Stier, P.: Will a perfect model agree with perfect observations? The impact of spatial sampling, Atmos. Chem. Phys., 16, 6335–6353, doi:10.5194/acp-16-6335-2016, 2016a.

Schutgens, N., Partridge, D., and Stier, P.: The importance of temporal collocation for the evaluation of aerosol models with observations, Atmos. Chem. Phys., 16, 1065–1079, doi:10.5194/acp-16-1065-2016, 2016b.

Schutgens, N., Tsyro, S., Gryspeerdt, E., Goto, D., Weigum, N., Schulz, M., and Stier, P.: On the spatio-temporal representativeness of observations, Atmos. Chem. Phys., 17, 9761–9780, doi:10.5194/acp-17-9761-2017, 2017.

Seinfeld, J. H., Bretherton, C., Carslaw, K. S., Coe, H., DeMott, P. J., Dunlea, E. J., Feingold, G., Ghan, S., Guenther, A. B., Kahn, R., Kraucunas, I., Kreidenweis, S. M., Molina, M. J., Nenes, A., Penner, J. E., Prather, K. A., Ramanathan, V., Ramaswamy, V., Rasch, P. J., Ravishankara, A. R., Rosenfeld, D., Stephens, G., and Wood, R.: Improving our fundamental understanding of the role of aerosol-cloud interactions in the climate system, Proc. Natl. Acad. Sci., 113, 5781–5790, doi:10.1073/pnas.1514043113, 2016.

Spracklen, D. V. and Rap, A.: Natural aerosol-climate feedbacks suppressed by anthropogenic aerosol, Geophys. Res. Lett., 40, 5316–5319, doi:10.1002/2013GL057966, 2013.

Stocker, T. F., Qin, D., Plattner, G. K., Tignor, M., Allen, S. K., Boschung, J., Nauels, A., Xia, Y., Bex, V., and Midgley, P. M.: Summary for Policymakers, in: Climate Change 2013: The Physical Science Basis. Contribution of Working Group I to the Fifth Assessment Report of the Intergovernmental Panel on Climate Change, edited by Stocker, T. F., Qin, D., Plattner, G. K., Tignor, M., Allen, S. K., Boschung, J., Nauels, A., Xia, Y., Bex, V., and Midgley, P. M., Cambridge University Press, Cambridge, United Kingdom and New York, NY, USA, 2013.

Tatzelt, C., Henning, S., Tummon, F., Hartmann, M., Baccarini, A., Welti, A., Lehtipalo, K. and Schmale, J.: Cloud Condensation Nuclei number concentrations over the Southern Ocean during the austral summer of 2016/2017, Version 1.0 Data set, doi:10.5281/zenodo.2636765, 2019.

Tett, S. F. B., Rowlands, D. J., Mineter, M. J., and Cartis, C.: Can Top-Of-Atmosphere Radiation Measurements Constrain Climate Predictions? Part II: Climate Sensitivity, J. Climate., 26, 9367–9383, doi:10.1175/JCLI-D-12-00596.1, 2013.

562 Turnock, S. T., Spracklen, D. V., Carslaw, K. S., Mann, G. W., Woodhouse, M. T., Forster, P. M., Haywood, J.,
563 Johnson, C. E., Dalvi, M., Bellouin, N., and Sanchez-Lorenzo, A.: Modelled and observed changes in
564 aerosols and surface solar radiation over Europe between 1960 and 2009, Atmos. Chem. Phys., 15, 13
565 457—-13 513, doi:10.5194/acpd-15-13457-2015, 2015.
566
567 van der Werf, G. R., Randerson, J. T., Giglio, L., Collatz, G. J., Mu, M., Kasibhatla, P. S., Norton, D. C., DeFries,
568 R. S., Jin, Y., and van Leeuwen, T. T.: Global fire emissions and the contribution of deforestation,
569 savanna, forest, agricultural, and peat fires (1997-2009), Atmos. Chem. Phys., 10, 11 707–11 735,
570 doi:10.5194/acp-10-11707-2010, 2010.
571
572 Walters, D. N., Williams, K. D., Boutle, I. A., Bushell, A. C., Edwards, J. M., Field, P. R., Lock, A. P., Morcrette, C.
573 J., Stratton, R. A., Wilkinson, J. M., Willett, M. R., Bellouin, N., Bodas-Solcedo, A., Brooks, M. E., Copsey,
574 D., Earnshaw, P. D., Hardiman, S. C., Harris, C. M., Levine, R. C., MacLachlan, C., Manners, J. C., Matin,
575 G. M., Milton, S. F., Palmer, M. D., Roberts, M. J., Rosriguez, J. M., Tennant, W. J., and Vidale, P. L.: The
576 Met Office Unified Model Global Atmosphere 4.0 and JULES Global Land 4.0 configurations, Geosci.
577 Mod. Dev., 7, 361–386, doi:10.5194/gmd-7-361-2014, 2014.
578
579 Watson-Paris, D., Bellouin, N., Deaconu, L., Schutgens, N., Yoshioka, M., Regayre, L.A., Pringle, K.J., Johnson,
580 J.S., Smith, C.S., Carslaw, K.S. and Stier, P.:Constraining uncertainty in aerosol direct forcing, Geophys.
581 Res. Lett., 47, 9, e2020GL087141, doi:10.1029/2020GL087141, 2020.
582
583 Weigum, N., Schutgens, N., and Stier, P.: Effect of aerosol subgrid variability on aerosol optical depth and cloud
584 condensation nuclei: implications for global aerosol modelling, Atmos. Chem. Phys., 16, 13 619–13 639,
585 doi:10.5194/acp-16-13619-2016, 2016.
586
587 West, R. E. L., Stier, P., Jones, A., Johnson, C. E., Mann, G. W., Bellouin, N., Partridge, D. G., and Kipling, Z.:
588 The importance of vertical velocity variability for estimates of the indircet aerosol effects, Atmos. Chem.
589 Phys., 14, 6369–6393, doi:10.5194/acp-14-6369-2014, 2014.
590
591 Wilcox, L. J., Highwood, E. J., Booth, B. B. B., and Carslaw, K. S.: Quantifying sources of inter-model diversity in
592 the cloud albedo effect, Geophys. Res. Lett., 42, 1568–1575, doi:10.1002/2015GL063301, 2015.
593
594 Williamson, D., Goldstein, M., Allison, L., Blaker, A., Challenor, P., Jackson, L., and Yamazaki, K.: History
595 matching for exploring and reducing climate model parameter space using observations and a large
596 perturbed physics ensemble, Clim. Dyn., 41, 1703–1729, doi:10.1007/s00382-013-1896-4, 2013.
597
598 Woodward, S.: Modeling the atmospheric life cycle and radiative impact of mineral dust in the Hadley Centre
599 climate model, J. Geo. Res., 106, 18 155–18 166, doi:10.1029/2000JD900795, 2001.
600
601 Yoshioka, M., Regayre, L. A., Pringle, K. J., Johnson, J. S., Mann, G. W., Partridge, D., Stier, P., Kipling, Z.,
602 Bellouin, N., Sexton, D. M. H ., Lister, G. M. S., Browse, J., Booth, B. B. B., Johnson, C. E., Johnson, B.,
603 Mollard, J. D. P., and Carslaw, K. S.: Ensembles of global climate model variants for the quantification and
604 constraint of uncertainty in aerosols and their radiative forcing, J. Adv. Model. Earth Syst., 11, 3728-3754,
605 doi:10.1029/2019MS001628, 2019.
606
607 Zhang, S., Wang, M., Ghan, S., Ding, A., Wang, H., Zhang, K., Neubauer, D., Lohmann, U., Ferrachat, S.,
608 Takeamura, T., Gettleman, A., Morrison, H., Lee, Y. H., Shindell, D. T., Partridge, D. G., Stier, P., Kipling,
609 Z., and Fu, C.: On the characteristics of aerosol indirect effect based on dynamic regimes in climate
610 models, Atmos. Chem. Phys., 16, 2765–2783, doi:10.5194/acp-16-2765-2016, 2016.
611